UV-active plasmons in alkali and alkaline-earth intercalated graphene

Despoja, Vito; Marušić, Leonardo

Source / Izvornik: **Physical Review B, 2018, 97**

Journal article, Published version
Rad u časopisu, Objavljena verzija rada (izdavačev PDF)

https://doi.org/10.1103/PhysRevB.97.205426

PHYSICAL REVIEW B **97**, 205426 (2018)

UV-active plasmons in alkali and alkaline-earth intercalated graphene

V. Despoja[1,2,*] and L. Marušić[3,†]
[1]*Institut za fiziku, Bijenička 46, 10000 Zagreb, Croatia*
[2]*Department of Physics, University of Zagreb, Bijenička 32, HR-10000 Zagreb, Croatia*
[3]*Maritime Department, University of Zadar, M. Pavlinovića 1, HR-23000 Zadar, Croatia*

(Received 2 March 2018; revised manuscript received 25 April 2018; published 16 May 2018)

The interband π and $\pi + \sigma$ plasmons in pristine graphene and the Dirac plasmon in doped graphene are not applicable, since they are broad or weak, and weakly couple to an external longitudinal or electromagnetic probe. Therefore, the *ab initio* density functional theory is used to demonstrate that the chemical doping of the graphene by the alkali or alkaline-earth atoms dramatically changes the poor graphene excitation spectrum in the ultraviolet frequency range (4–10 eV). Four prominent modes are detected. Two of them are the intralayer plasmons with square-root dispersion, characteristic of the two-dimensional modes. The remaining two are the interlayer plasmons, very strong in the long-wavelength limit but damped for larger wave vectors. The optical absorption calculations show that the interlayer plasmons are both optically active, which makes these materials suitable for small-organic-molecule sensing. This is particularly intriguing because the optically active two-dimensional plasmons have not been detected in other materials.

DOI: 10.1103/PhysRevB.97.205426

Extensive research of electronic excitations in graphene showed the existence of several two-dimensional (2D) plasmon modes: the intraband (Dirac) plasmon existing only in doped graphene [1–6], and the interband plasmons, which exist in pristine and doped graphene and originate from the interband electron-hole transition between the π and π^* bands and between the π and σ^* bands [3,7–10]. These investigations also showed that the interband π and $\pi + \sigma$ plasmons are broad and weak resonances, so their interaction with the external longitudinal or electromagnetic probes is weak as well, which makes them inadequate for most practical applications. The "tunable" Dirac plasmon in doped graphene is also weak (for experimentally feasible doping) and, in addition to that, it does not couple to an incident electromagnetic field directly. In the systems proposed so far, light could be coupled to the Dirac plasmon only indirectly, e.g., by using metallic tips, gratings, or prisms, or by arranging graphene into nanoribbons [4,5,11], which is in most cases not easy to fabricate. Also, such indirect coupling additionally reduces the intensity of the plasmon, thus reducing the efficiency of its application.

The alkali or alkaline-earth intercalated graphene is relatively easy to fabricate and offers a broader variety of plasmons, both intraband and (especially) interband. Such systems have recently been extensively studied, both theoretically and experimentally [12–18], but the attention has not been on the electronic excitations. Intercalating any alkali or alkaline-earth metal to a single graphene layer causes the natural doping of the graphene and results in the formation of two quasi-two-dimensional (q2D) plasmas. This supports the existence of two 2D intraband plasmons, acoustic and Dirac, with frequencies up to 4 eV [19], as well as several interband and even interlayer modes occurring at higher frequencies. Some of these modes are optically active and some of them can be manipulated by doping, which opens possibilities for their application in various fields, such as plasmonics, photonics, transformation optics, optoelectronics, light emitters, detectors, and photovoltaic devices [20–29]. Moreover, tunable 2D plasmons could be very useful in the area of chemical or biological sensing [20,30–32], which is one of our main suggestions for the potential application of the results of this research. In addition to that we study the interlayer interband excitations and demonstrate that they are not only plasmons but optically active plasmons, as pointed out in the title to emphasize the importance of these modes. Unlike the widely studied infrared Dirac plasmon or UV π plasmon in graphene, these plasmons can be excited directly by light.

We performed calculations for several alkali and alkaline-earth metals, with different coverages, and found that the effects which are the focus of this paper are valid for all of them. In all these cases, in addition to the graphene π and σ bands, there are also the π and σ bands of the intercalated metal. This opens possibilities for various electron-hole (*e*-h) transitions which may be the origins of the interband plasmons. We limit our investigation to the frequencies between 4 and 10 eV (the UV region), where the dominant interband plasmons occur, and identify four significant modes within this range. Two of them are not very well defined in the long-wavelength limit but they exist at larger wave vectors as well, and show the square-root dispersion characteristic of the surface and 2D modes. These modes are the intralayer modes, one located in the graphene layer and the other located in the metallic layer. The other two are very prominent in the long-wavelength limit, but at higher wave vectors their intensities rapidly decrease, which makes them potentially interesting for optical applications [11,20,21,33]. Their dispersions are different from those typical for the 2D modes, indicating that they are different

---

[*] vito@phy.hr

[†] lmarusic@unizd.hr

from the usual 2D plasmons. Detailed inspection (including retardation, i.e., finite speed of light, and tensoric response) shows that they are dipolar interlayer modes (the electric field they produce oscillates perpendicular to the crystal plane), i.e., optically active q2D plasmons, contrary to the widely studied q2D plasmons which produce electric field parallel to the crystal plane and are not optically active. The extensively studied graphene π and $\pi+\sigma$ modes are optically active, but in the long-wavelength limit ($Q \to 0$) they are not plasmons but electron-hole excitations [9]. The optical plasmons in the intercalated graphene fit the small organic molecules' optical absorption peaks (e.g., bright excitons at 5.2, 6.3, and 7 eV in anthracene, fullerene, and benzene, respectively) and therefore can be applied as chemical detectors operating in the UV frequency region.

The theoretical formulation of the electronic response in various q2D systems has already been presented [3,34–36], so here we only point out some details of the calculation important for the understanding of the result we want to present. We define the electron-energy-loss spectroscopy (EELS) local spectral function as the imaginary part of the excitation propagator,

$$S_{z_0}(\mathbf{Q},\omega) = -\mathrm{Im}D_{z_0}(\mathbf{Q},\omega), \tag{1}$$

where

$$D_{z_0}(\mathbf{Q},\omega) = W^{\mathrm{ind}}_{\mathbf{G}_\parallel=0}(\mathbf{Q},\omega,z_0,z_0). \tag{2}$$

The $S_{z_0}(\mathbf{Q},\omega)$ is also proportional to the probability density for the parallel momentum transfer $\mathbf{Q}=(Q_x,Q_y)$ and the energy loss ω of the reflected electron in the reflection electron-energy-loss spectroscopy (REELS) [37]. The induced dynamically screened Coulomb interaction is $W^{\mathrm{ind}} = v^{\mathrm{2D}} \otimes \chi \otimes v^{\mathrm{2D}}$, where $v^{\mathrm{2D}} = \frac{2\pi}{Q}e^{-Q|z-z'|}$ is the 2D Fourier transform of the bare Coulomb interaction and $\otimes = \int_{-L/2}^{L/2} dz$ [38]. The response function is obtained as the solution of the matrix Dyson equation $\hat{\chi} = \hat{\chi}^0 + \hat{\chi}^0\hat{v}^{\mathrm{2D}}\hat{\chi}$ in the reciprocal-space plane-wave basis $\mathbf{G}=(\mathbf{G}_\parallel,G_z)$. The noninteracting electrons response matrix is $\hat{\chi}^0 = \frac{2}{\Omega}\sum_{i,j}(f_i - f_j)/(\omega + i\eta + E_i - E_j)\rho_{\mathbf{G},ij}\rho^*_{\mathbf{G}',ij}$, where f_i is the Fermi-Dirac distribution, $\rho_{\mathbf{G},ij}$ are charge vertices [3], Ω is the normalization volume, and $i=(n,\mathbf{K})$ and $j=(m,\mathbf{K}+\mathbf{Q})$ are Kohn-Sham-Bloch states. The Coulomb interaction with the surrounding supercells in the superlattice arrangement is excluded, as described in detail in Ref. [34].

In this paper we study LiC$_2$, LiC$_6$, CaC$_6$, and CsC$_8$ crystal slabs, which consist of two parallel atomic layers (one metallic and one carbon) separated by distance d. The metallic atoms occupy hollow sites and form 1×1, $\sqrt{3}\times\sqrt{3}$, $\sqrt{3}\times\sqrt{3}$, and 2×2 superlattices, respectively, corresponding to the graphene hexagonal lattice. To calculate the Kohn-Sham (KS) wave functions $\phi_{n\mathbf{K}}$ and energy levels $E_{n\mathbf{K}}$, i.e., the band structure, of the slabs, we use the plane-wave self-consistent field (PWSCF) DFT code within the QUANTUM ESPRESSO (QE) package [39]. The core-electron interaction is approximated by the norm-conserving pseudopotentials [40], and the exchange correlation (XC) potential by the Perdew-Zunger local density approximation (LDA) [41]. For the slab unit cell constant we use the graphene value of $a_{uc} = 4.651$ a.u. [42], and we separate the slabs by $L = 5a_{uc} = 23.255$ a.u. We performed structural optimization calculations for all systems until the maximum atom-atom force was reduced below 0.002 eV/Å. The equilibrium separations between the metallic and carbon layers within a slab for these four systems are $d = 4.1$ a.u. (2.17 Å), 3.28 a.u. (1.74 Å), 4.46 a.u. (2.36 Å), and 5.8 a.u. (3.08 Å), respectively, which is consistent with those in Refs. [18,43]. Even though all the structures are theoretically stable, the only one that has been experimentally synthesized (with certainty) is LiC$_6$ [18]. For all the others (LiC$_6$, CaC$_6$, and CsC$_8$), there are indications of their existence, but it has not been confirmed. In particular, there are indications that it may be possible to achieve Li coverage larger than $\sqrt{3}\times\sqrt{3}$, even up to 1×1 [44]. On the other hand, for larger atoms the coverage is smaller and this is why for the Cs intercalation we use 2×2, which seems to be experimentally stable [45]. Finally, in this

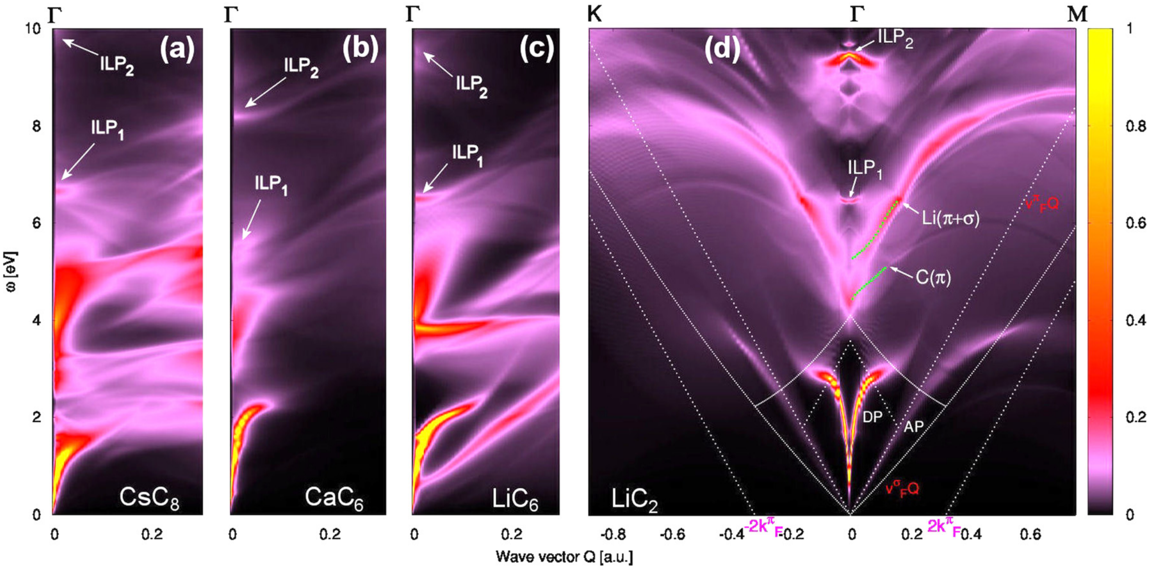

FIG. 1. The intensity of the electronic excitations in (a) CsC$_8$, (b) CaC$_6$, (c) LiC$_6$, and (d) LiC$_2$. The white and green dotted lines in (d) show the boundaries of the e-h excitation gaps for the graphene π bands around the Dirac point and the Li σ bands around the Γ point, respectively.

investigation we want to cover a wider class of intercalates, regardless of whether they have been synthesized or not, with the hope that at least some of them will be fabricated in the future, and that they will manifest desirable plasmonics. Our reference frame is chosen so that the graphene layer is positioned at $z = 0$, and the metallic layer is at $z = d$. The ground-state electronic densities of the slabs are calculated by using the $12 \times 12 \times 1$ Monkhorst-Pack K-point mesh [46] of the first Brillouin zone (BZ). For the plane-wave cutoff energy we choose 50 Ry (680 eV). The Fermi levels of these systems (measured from the Dirac point, i.e., from the pristine graphene Fermi level) are $E_F = 1.78, 1.55, 1.375,$ and 1.24 eV, respectively. For the response matrix $\hat{\chi}^0$ calculation in the long-wavelength ($Q < 0.01$ a.u.) limit we use $601 \times 601 \times 1$ K-point mesh and the damping parameter $\eta = 10$ meV, while for the larger Qs we use $201 \times 201 \times 1$ K-point mesh sampling and $\eta = 30$ meV. In all cases the band summation is performed over 30 bands and the perpendicular crystal local field energy cutoff is 10 Ry (136 eV), which corresponds with $23G_z$ wave vectors. The temperature used in the noninteracting electrons response matrix $\hat{\chi}^0$ calculations is $T = 10$ meV (116 K).

Figures 1(a)–1(d) show the excitation spectra in CsC_8, CaC_6, LiC_6, and LiC_2 slabs, respectively, calculated from Eq. (1). The spectral intensities are shown as functions of ω and Q, using the color scheme, which enables us to see the dispersions of the modes. We can see that, in addition to the well-known modes present in the doped graphene (Dirac (DP) and π (C(π)) plasmon [3]), there are a few other modes, strong in the long-wavelength limit (indicating their optical activity) and more pronounced in the systems with higher electronic doping, especially for LiC_6 and LiC_2. Therefore, we put emphasis on the system with the highest doping, i.e., the LiC_2. Figure 1(d) shows the intensities of the electronic excitations in the ΓM and ΓK directions for the LiC_2. The spectra in these two directions are very similar, so here we focus only on the ΓM direction. At lower frequencies (up to 4 eV) we can see the intraband q2D plasmons, which have already been discussed in detail for LiC_2 [19]. At frequencies between 4 and 10 eV we can see four significant interband modes (denoted as C(π), Li($\pi + \sigma$), ILP_1, and ILP_2), two with the square-root dispersion, characteristic of the q2D systems, which exist for the larger wave vectors as well, and the other two which are strongly damped for larger wave vectors. These modes, which exist in all these systems (at similar frequencies), are the focus of this paper. To understand them we explore the band structure and the spectra of electronic excitations in the LiC_2 in more detail. However, our conclusions about the origins and characteristics of the modes obtained for the LiC_2 are valid for the other three systems as well.

Figures 2(a) and 2(b) show spectra $S(\omega)$ for the LiC_2 for various wave vectors Q (denoted in graphs) in the ΓM direction. Figure 2(b) also contains the spectra of the n-doped graphene (dashed red lines), with the same doping as in the LiC_2 ($E_F = 1.78$ eV), for comparison. The doped graphene spectra show two modes, the very prominent intraband Dirac plasmon, roughly matching the LiC_2 Dirac plasmon, and the interband π plasmon around 5 eV, which is very weak due to heavy doping. In the LiC_2 spectra, in addition to the already described q2D intraband acoustic and Dirac plasmon (AP and DP) [19], we can notice a barely visible broad peak between 4.5 and 5 eV, which corresponds with the graphene π plasmon, plus three other modes which cannot be related to any of the graphene modes. This means that these modes are either the lithium q2D intralayer modes, or the interlayer modes, which represent charge oscillations perpendicular to the crystal plane. Therefore, Li intercalation not only donates electrons to the graphene π cone (enabling the Dirac plasmon) but also drastically modifies interband plasmonics. Acoustic plasmons can appear in graphene composites which are not intercalated by alkali metals (e.g., acoustic plasmon and various hybridized plasmonic/phononic modes in graphene/sapphire/graphene composites [47], but these graphene/insulator/graphene composites do not support the intriguing interband plasmons studied here).

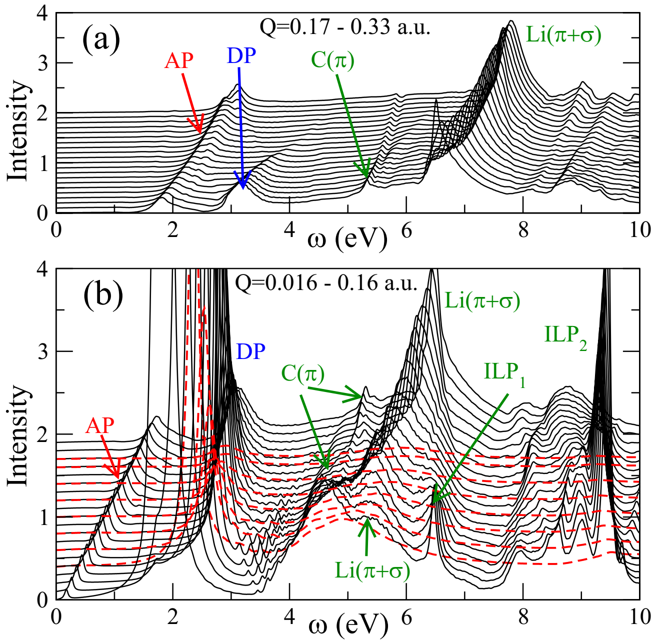

FIG. 2. Spectra of the electronic excitations in LiC_2 for the wave vectors (a) $Q = 0.17-0.33$ a.u. and (b) $Q = 0.016-0.16$ a.u. in the ΓM direction (solid black lines). (b) Comparison with the doped graphene spectra (dashed red lines) with the matching Fermi level.

In order to determine the properties (the origin) of particular interband plasmons we should bring them into connection with the corresponding single-particle electron-hole transitions. Figure 3(a) shows the band structure of the LiC_2 slab, with the color scheme indicating the predominant origins of particular bands. Blue and turquoise indicate predominant lithium π and σ orbitals, respectively, while red and pink indicate predominant graphene π and σ orbitals, respectively. The arrows indicate the e-h transitions which are the potential origins of the four modes. However, since the transition energies are very similar, it is impossible to reach definite conclusions about the origins of the particular modes from the band structure itself. Figure 3(b) shows the imaginary (thick solid black line) and real (thick dashed black line) parts of the excitation propagator (2) in the LiC_2 for several characteristic wave vectors Q. The thin red line is the unscreened (single-particle) spectrum obtained by replacing χ with χ^0 in W^{ind} used in Eq. (1). By comparing these three lines we can distinguish the collective

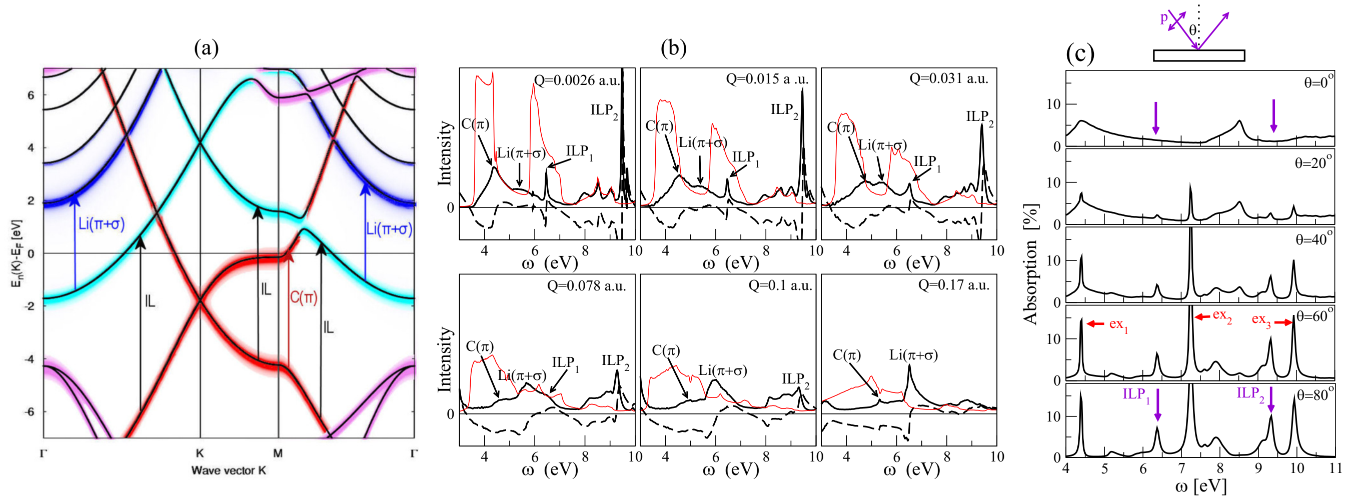

FIG. 3. (a) The band structure of the LiC_2, with the color scheme indicating the predominant origins of particular bands (blue, Li(π); turquoise, Li(σ); pink, C(σ); red, C(π)). (b) Development of the interband plasmons with the increase of the wave vector. Thick solid black lines, ImD; thick dashed black lines, ReD; thin red lines, spectra of the single-particle excitations only. (c) Angle-resolved optical absorption spectra in LiC_2, in ultraviolet frequency range.

modes from the single-particle excitations. Furthermore, comparing the frequencies of these excitations with the transitions in the band structure in Fig. 3(a) can help us identify the origins of some of the modes.

In the unscreened spectra (thin red lines) we can see two prominent peaks, one around 4 eV which exists for all wave vectors, and the other around 6 eV which disappears for larger Q. This indicates that the first one is the origin of the modes denoted as C(π) and Li($\pi+\sigma$), while the second one is the origin of the remaining two modes (IL_1 and IL_2). Further analysis consists of applying the p and n doping to our system (i.e., changing the position of the Fermi level and causing some occupied bands to become unoccupied, and vice versa), and omitting particular bands from the calculation of the response function χ^0, to determine the exact role of each band. By doing that, we found out that the first peak in the single-particle spectra is actually an overlap of two peaks. One is coming from the transition between the π and π^* graphene bands around the M point [red arrow in Fig. 3(a)], and that one is the origin of the mode denoted as C(π), i.e., the graphene π plasmon. The other is coming from the transition between the σ and π lithium bands around the Γ point [blue arrow in Fig. 3(a)], and that one is the origin of the mode denoted as Li($\pi+\sigma$), i.e., the lithium $\pi+\sigma$ plasmon. The second peak in the single-particle spectra comes from the transitions between the graphene π bands and the lithium σ bands [black arrows in Fig. 3(a)], and it is the origin of the remaining two modes, denoted as IL_1 and IL_2. Their dispersion is not square-root like, which is the consequence of their interlayer nature. All the presented spectra are calculated for the probe positioned at $z_0=L/2$, but we can change the position of the probe and monitor the changes in the spectra to determine the symmetry of the particular modes. By doing that we confirmed that one of the peaks (IL_1) is even, while the other one (IL_2) is odd.

Contrary to the intralayer plasmons C(π) and Li($\pi+\sigma$), the interlayer plasmons IL_1 and IL_2 are sharp, well-defined resonances which could be especially suitable for the sensing of small organic molecules with excitonic spectra in the UV frequency range. However, the crucial question is: Can the IL_1 and IL_2 plasmons be excited by an external electromagnetic field, i.e, are they optically active? If that is the case, then it seems that the intercalated graphene may become the technologically simplest platform for biosensing. In the systems proposed so far, light could be coupled to plasmon resonances only indirectly, e.g., by using the metallic nanoparticles, gratings, or prisms, or by arranging graphene into nanoribbons, which is much more difficult to fabricate. Another exciting aspect of this issue is that the optically active q2D plasmons have not been discovered in other systems. In order to answer this crucial question we performed a sophisticated angle-resolved optical absorption calculation which includes the retardation and the tensoric character of the LiC_2 dynamical response [48]. The mathematical formulation of the electromagnetic wave scattering and the expression for the angle-resolved optical absorption in two-dimensional crystals are presented in the Supplemental Material [49].

Figure 3(c) shows the absorption of p polarized light in the LiC_2, as a function of the incident light with the frequency ω and angle θ (as sketched), calculated by using (S16) and (S17) presented in the Supplemental Material [49]. For the normal incidence ($\theta=0^\circ$) the electric field is parallel with the crystal plane and there are no peaks corresponding to IL_1 and IL_2. However, as the incident angle increases, the IL_1 and IL_2 peaks appear, and finally for the almost grazing incidence ($\theta=80^\circ$), i.e., for the the electrical field almost perpendicular to the crystal plane, they become very intensive. This undoubtedly confirms not only that these modes are optically active, but also their interlayer character. The grazing spectra show some additional peaks (ex_1, ex_2, and ex_3) which do not appear in the EELS spectra, i.e., which cannot be excited by an external longitudinal probe, which means that they are probably not plasmons but UV-active excitons.

In the remaining three systems presented in this paper, the electronic doping is weaker than in the LiC_2, which has two important consequences. First, the two interlayer plasmons are not nearly as strong and sharp as they are in the LiC_2, but they still exist and are still optically active in the UV region. Second, due to the weaker doping the Fermi level is lower (with respect to the LiC_2 Fermi level) by 0.23 eV for LiC_6, 0.405 eV for CaC_6, and 0.54 eV for CsC_8. Considering that the plateau in the graphene π^* band is only 0.1–0.2 eV below the LiC_2 Fermi level, this means that in the three other systems that plateau is unoccupied, which makes the graphene π plasmon much stronger. Therefore, by changing the doping (by changing the dopant or the coverage, or by applying the gate voltage) we can tune these modes, i.e., increase or decrease their intensities.

In conclusion, we showed that doping the graphene by the alkali or alkaline-earth atoms dramatically modifies the graphene plasmonics, especially in UV parts of the spectra, where we obtain four interband plasmons. This effect is the strongest in the full coverage lithium-doped graphene (LiC_2), due to the highest doping. Two of the modes, not very strong in the long-wavelength limit, exist for larger wave vectors, with the square-root dispersion characteristic of the 2D plasmons. They turned out to be the intralayer modes, one within the graphene layer (the well-known graphene π plasmon), and the other within the intercalated metal layer. The other two plasmons ILP_1 and ILP_2 are strong and sharp in the long-wavelength limit, but damped for the larger wave vectors. They turned out to be the interlayer optically active plasmons; i.e., they couple directly to the electromagnetic field. Such unusual and poorly explored optically active 2D plasmons can be used as an efficient sensor in chemical sensing and biosensing.

This work was supported by the QuantiXLie Centre of Excellence, a project co-financed by the Croatian Government and European Union through the European Regional Development Fund: the Competitiveness and Cohesion Operational Programme (Grant No. KK.01.1.1.01.0004). Computational resources were provided by the Donostia International Physic Center (DIPC) computing center.

---

[1] E. H. Hwang and S. Das Sarma, Phys. Rev. B **75**, 205418 (2007); **80**, 205405 (2009).

[2] E. H. Hwang, R. Sensarma, and S. Das Sarma, Phys. Rev. B **82**, 195406 (2010).

[3] V. Despoja, D. Novko, K. Dekanić, M. Šunjić, and L. Marušić, Phys. Rev. B **87**, 075447 (2013).

[4] H. Yan, T. Low, W. Zhu, Y. Wu, M. Freitag, X. Li, F. Guinea, P. Avouris, and F. Xia, Nat. Photonics **7**, 394 (2013).

[5] Z. Fei, G. O. Andreev, W. Bao, L. M. Zhang, A. S. McLeod, C. Wang, M. K. Stewart, Z. Zhao, G. Dominguez, M. Thiemens, M. M. Fogler, M. J. Tauber, A. H. Castro-Neto, C. N. Lau, F. Keilmann, and D. N. Basov, Nano Lett. **11**, 4701 (2011).

[6] M. Jablan, H. Buljan, and M. Soljačić, Phys. Rev. B **80**, 245435 (2009).

[7] A. Politano, I. Radović, D. Borka, Z. L. Mišković, and G. Chiarello, Carbon **96**, 91 (2016).

[8] A. Politano, I. Radović, D. Borka, Z. L. Mišković, H. K. Yu, D. Farías, and G. Chiarello, Carbon **114**, 70 (2017).

[9] D. Novko, V. Despoja, and M. Šunjić, Phys. Rev. B **91**, 195407 (2015).

[10] T. Eberlein, U. Bangert, R. R. Nair, R. Jones, M. Gass, A. L. Bleloch, K. S. Novoselov, A. Geim, and P. R. Briddon, Phys. Rev. B **77**, 233406 (2008).

[11] C. Vacacela Gomez, M. Pisarra, M. Gravina, J. M. Pitarke, and A. Sindona, Phys. Rev. Lett. **117**, 116801 (2016).

[12] A. Kumar, A. L. M. Reddy, A. Mukherjee, M. Dubey, X. Zhan, N. Singh, L. Ci, W. E. Billups, J. Nagurny, G. Mital, and P. M. Ajayan, ACS Nano **5**, 4345 (2011).

[13] S.-L. Yang, J. A. Sobota, C. A. Howard, C. J. Pickard, M. Hashimoto, D. H. Lu, S.-K. Mo, P. S. Kirchmann, and Z.-X. Shen, Nat. Commun. **5**, 3493 (2014).

[14] N. M. Caffrey, L. I. Johansson, C. Xia, R. Armiento, I. A. Abrikosov, and C. Jacobi, Phys. Rev. B **93**, 195421 (2016).

[15] S. Ichinokura, K. Sugawara, A. Takayama, T. Takahashi, and S. Hasegawa, ACS Nano **10**, 2761 (2016).

[16] K. Li, X. Feng, W. Zhang, Y. Ou, L. Chen, Ke. He, Li-Li Wang, L. Guo, G. Liu, Qi-Kun Xue, and X. Ma, Appl. Phys. Lett. **103**, 062601 (2013).

[17] M. Khantha, N. A. Cordero, L. M. Molina, J. A. Alonso, and L. A. Girifalco, Phys. Rev. B **70**, 125422 (2004).

[18] P. Pervan, P. Lazić, M. Petrović, I. Šrut Rakić, I. Pletikosić, M. Kralj, M. Milun, and T. Valla, Phys. Rev. B **92**, 245415 (2015).

[19] L. Marušić and V. Despoja, Phys. Rev. B **95**, 201408(R) (2017).

[20] F. Bonaccorso, Z. Sun, T. Hasan, and A. C. Ferrari, Nat. Photonics **4**, 611 (2010).

[21] A. Vakil and N. Engheta, Science **332**, 1291 (2011).

[22] W. Hua-Qiang, L. Chang-Yang, L. Hong-Ming, and Q. He, Chin. Phys. B **22**, 098106 (2013).

[23] A. Pospischil, M. M. Furchi, and T. Mueller, Nat. Nanotechnol. **9**, 257 (2014).

[24] J. S. Ross, P. Klement, A. M. Jones, N. J. Ghimire, J. Yan, D. G. Mandrus, T. Taniguchi, K. Watanabe, K. Kitamura, W. Yao, D. H. Cobden, and X. Xu, Nat. Nanotechnol. **9**, 268 (2014).

[25] F. H. L. Koppens, T. Mueller, P. Avouris, A. C. Ferrari, M. S. Vitiello, and M. Polini, Nat. Nanotechnol. **9**, 780 (2014).

[26] S. Jo, N. Ubrig, H. Berger, A. B. Kuzmenko, and A. F. Morpurgo, Nano Lett. **14**, 2019 (2014).

[27] O. Lopez-Sanchez, E. Alarcon Llado, V. Koman, A. Fontcuberta i Morral, A. Radenovic, and A. Kis, ACS Nano **8**, 3042 (2014).

[28] C.-H. Lee, G.-H. Lee, A. M. van der Zande, W. Chen, Y. Li, M. Han, X. Cui, G. Arefe, C. Nuckolls, T. F. Heinz, J. Guo, J. Hone, and P. Kim, Nat. Nanotechnol. **9**, 676 (2014).

[29] B. W. H. Baugher, H. O. H. Churchill, Y. Yang, and P. Jarillo-Herrero, Nat. Nanotechnol. **9**, 262 (2014).

[30] T. Low and P. Avouris, ACS Nano **8**, 1086 (2014).

[31] L. Britnell, R. M. Ribeiro, A. Eckmann, R. Jalil, B. D. Belle, A. Mishchenko, Y. J. Kim, R. V. Gorbachev, T. Georgiou, S. V. Morozov, A. N. Grigorenko, A. K. Geim, C. Casiraghi, A. H. C. Neto, and K. S. Novoselov, Science **340**, 1311 (2013).

[32] C. Zhu, D. Du, and Y. Lin, 2D Mater. **2**, 032004 (2015); A. Y. Zhu and E. Cubukcu, *ibid.* **2**, 032005 (2015).

[33] T. Stauber and H. Kohler, Nano Lett. **16**, 6844 (2016).

[34] V. Despoja, Z. Rukelj, and L. Marušić, Phys. Rev. B **94**, 165446 (2016).

[35] V. Despoja, D. J. Mowbray, D. Vlahović and L. Marušić, Phys. Rev. B **86**, 195429 (2012).

[36] V. Despoja, K. Dekanić, M. Šunjić, and L. Marušić, Phys. Rev. B **86**, 165419 (2012).

[37] Z. L. Wang and J. M. Cowley, Surf. Sci. **193**, 501 (1988).

[38] L. Marušić and M. Šunjić, Phys. Scr. **63**, 336 (2001).

[39] P. Giannozzi, S. Baroni, N. Bonini, M. Calandra, R. Car, C. Cavazzoni, D. Ceresoli, G. L. Chiarotti, M. Cococcioni, I. Dabo *et al.*, J. Phys.: Conden. Matter **21**, 395502 (2009).

[40] N. Troullier and J. L. Martins, Phys. Rev. B **43**, 1993 (1991).

[41] J. P. Perdew and A. Zunger, Phys. Rev. B **23**, 5048 (1981).

[42] R. Saito, G. Dresselhaus, and M. S. Dresselhaus, *Physical Properties of Carbon Nanotubes* (Imperial College Press, London, 1998).

[43] D. Novko, Nano Lett. **17**, 6991 (2017).

[44] J. Halle, N. Neel, and J. Kroger, J. Phys. Chem. C **120**, 5067 (2016).

[45] M. Petrović, I. Šrut Rakić, S. Runte, C. Busse, J. T. Sadowski, P. Lazić, I. Pletikosić, Z.-H. Pan, M. Milun, P. Pervan, N. Atodiresei, R. Brako, D. Šokčević, T. Valla, T. Michely, and M. Kralj, Nat. Commun. **4**, 2772 (2013).

[46] H. J. Monkhorst and J. D. Pack, Phys. Rev. B **13**, 5188 (1976).

[47] V. Despoja, T. Djordjević, L. Karbunar, I. Radović, and Z. L. Mišković, Phys. Rev. B **96**, 075433 (2017).

[48] D. Novko, M. Šunjić, and V. Despoja, Phys. Rev. B **93**, 125413 (2016).

[49] See Supplemental Material at http://link.aps.org/supplemental/10.1103/PhysRevB.97.205426 for more details on computational methods for electromagnetic wave scattering and angle-resolved optical absorption in quasi-two-dimensional crystals.